



A direct vulnerable atherosclerotic plaque elasticity reconstruction method based on an original material-finite element formulation: theoretical framework.

Adeline Bouvier, Flavien Deleaval, Marvin M. Doyley, Saami K. Yazdani, Gérard Finet, Simon Le Floc'H, Guy Cloutier, Roderic I. Pettigrew, Jacques Ohayon

► To cite this version:

Adeline Bouvier, Flavien Deleaval, Marvin M. Doyley, Saami K. Yazdani, Gérard Finet, et al.. A direct vulnerable atherosclerotic plaque elasticity reconstruction method based on an original material-finite element formulation: theoretical framework.. *Physics in Medicine and Biology*, 2013, 58 (23), pp.8457-8476. 10.1088/0031-9155/58/23/8457 . hal-01017137

HAL Id: hal-01017137

<https://hal.science/hal-01017137v1>

Submitted on 25 Mar 2016

HAL is a multi-disciplinary open access archive for the deposit and dissemination of scientific research documents, whether they are published or not. The documents may come from teaching and research institutions in France or abroad, or from public or private research centers.

L'archive ouverte pluridisciplinaire **HAL**, est destinée au dépôt et à la diffusion de documents scientifiques de niveau recherche, publiés ou non, émanant des établissements d'enseignement et de recherche français ou étrangers, des laboratoires publics ou privés.



Published in final edited form as:

Phys Med Biol. 2013 December 7; 58(23): 8457–8476. doi:10.1088/0031-9155/58/23/8457.

A direct vulnerable atherosclerotic plaque elasticity reconstruction method based on an original material-finite element formulation: theoretical framework

Adeline Bouvier^{1,9}, Flavien Deleaval^{1,9}, Marvin M Doyley², Saami K Yazdani³, Gérard Finet⁴, Simon Le Floc'h⁵, Guy Cloutier⁶, Roderic I Pettigrew^{7,10}, and Jacques Ohayon^{1,8,10}

Jacques Ohayon: jacques.ohayon@imag.fr

¹Laboratory TIMC-IMAG/DyCTiM, UJF, CNRS UMR 5525, In³S, Grenoble, France

²Department of Electrical and Computer Engineering, University of Rochester, Rochester, NY, USA

³Department of Mechanical Engineering, University of South Alabama, Mobile, AL, USA

⁴Department of Hemodynamics and Interventional Cardiology, Hospices Civils de Lyon and Claude Bernard University Lyon1; INSERM Unit 886, Lyon, France

⁵Laboratory LMGC, CNRS UMR 5508, Université Montpellier II, Montpellier, France

⁶Laboratory of Biorheology and Medical Ultrasonics, University of Montreal Hospital Research Center (CRCHUM), Montréal, Québec, Canada

⁷Laboratory of Integrative Cardiovascular Imaging Science, National Institute of Diabetes Digestive and Kidney Diseases, National Institutes of Health, Bethesda, MD, USA

⁸University of Savoie, Polytech Annecy-Chambéry, Le Bourget du Lac, France

Abstract

The peak cap stress (PCS) amplitude is recognized as a biomechanical predictor of vulnerable plaque (VP) rupture. However, quantifying PCS *in vivo* remains a challenge since the stress depends on the plaque mechanical properties. In response, an iterative material finite element (FE) elasticity reconstruction method using strain measurements has been implemented for the solution of these inverse problems. Although this approach could resolve the mechanical characterization of VPs, it suffers from major limitations since (i) it is not adapted to characterize VPs exhibiting high material discontinuities between inclusions, and (ii) does not permit real time elasticity reconstruction for clinical use. The present theoretical study was therefore designed to develop a direct material-FE algorithm for elasticity reconstruction problems which accounts for material heterogeneities. We originally modified and adapted the extended FE method (Xfem), used mainly in crack analysis, to model material heterogeneities. This new algorithm was successfully applied to six coronary lesions of patients imaged *in vivo* with intravascular ultrasound. The results demonstrated that the mean relative absolute errors of the reconstructed Young's moduli obtained for the arterial wall, fibrosis, necrotic core, and calcified regions of the VPs decreased from

¹⁰Authors to whom any correspondence should be addressed.

⁹These two authors contributed equally to this work.

95.3±15.56%, 98.85±72.42%, 103.29±111.86% and 95.3±10.49%, respectively, to values smaller than $2.6 \times 10^{-8} \pm 5.7 \times 10^{-8}\%$ (i.e. close to the exact solutions) when including modified-Xfem method into our direct elasticity reconstruction method.

1. Introduction

Vulnerable atherosclerotic plaque (VP) rupture remains the leading cause of acute coronary syndrome (ACS), myocardial infarction and stroke (Lloyd-Jones *et al* 2010). Atherosclerotic lesions with a relatively large extracellular necrotic core and a thin fibrous cap infiltrated by macrophages are prone to be vulnerable to rupture (Virmani *et al* 2000). The rupture of the thin-cap fibroatheroma (TCFA) may lead to the formation of a thrombus causing the acute syndrome and possibly death (Virmani *et al* 2006). Because early detection of vulnerable atherosclerotic lesions is a crucial step in preventing risk of rupture and managing ACS and strokes, several intravascular imaging techniques have been developed (Vancraeynest *et al* 2011). These include intravascular ultrasound (IVUS) (Rioufol *et al* 2002, Carlier and Tanaka 2006), optical coherence tomography (OCT) (Jang *et al* 2002, Tearney *et al* 2008) and magnetic resonance imaging (IV-MRI) (Larose *et al* 2005, Briley-Saebo *et al* 2007). Diagnosis of high-risk atherosclerotic plaques remains problematic as the thickness of the fibrous cap alone is not a sufficient predictor of plaque stability (Virmani *et al* 2000, Ohayon *et al* 2008, Fleg *et al* 2012, Maldonado *et al* 2012).

Previous works have identified peak cap stress (PCS) amplitude as the biomechanical key predictor of vulnerability to rupture (Loree *et al* 1992, Ohayon *et al* 2001, Finet *et al* 2004). Quantifying PCS *in vivo* remains a challenge since such mechanical stress within the cap depends not only on the VP morphology, but also on the mechanical properties of the plaque components (Ohayon *et al* 2008). Although several methods have been developed to extract the spatial strain distributions (Doyley *et al* 2001, Wan *et al* 2001, de Korte *et al* 2002, Kim *et al* 2004, Maurice *et al* 2004), the complex geometries of atherosclerotic plaques inhibit direct translation into plaque mechanical properties.

Based on the estimation of the strain field inside the atherosclerotic lesion obtained from various intravascular imaging techniques, several studies have been performed to estimate vascular elasticity maps (Doyley 2012). Two types of approaches were proposed: direct (Zhu *et al* 2003, Kanai *et al* 2003, Guo *et al* 2010) or iterative (Doyley *et al* 2000, Oberai *et al* 2003, Baldewsing *et al* 2005, Le Floc'h *et al* 2009, Richards and Doyley 2011). Inspired by the work of Baldewsing *et al* (2005), Le Floc'h *et al* (2009) developed an elasticity reconstruction technique (termed iMOD for imaging Young's modulus) based on an original pre-conditioning step for the optimization process, and an approach combining a dynamic watershed segmentation method with a mathematical optimization procedure. The main advantage of this iterative method is its pre-conditioning step which automatically identifies the contours of all the components before the optimization process. Despite the effectiveness and robustness of the iMOD approach (Le Floc'h *et al* 2010, 2012), this algorithm does not permit real time elasticity reconstruction for clinical use since the resolution of the inverse elasticity problem remains time-consuming (several minutes) for high definition reconstruction elasticity maps. Zhu *et al* (2003) developed a direct computational finite element (FE) approach for fast Young's modulus reconstruction assuming constant

mechanical properties in each FE. However, the computational time performance of such a technique is clobbered by the rise in number of FE when considering highly heterogeneous anatomical atherosclerotic plaques. To overcome this limitation, Oberai *et al* (2003) proposed a material-FE elasticity reconstruction method in which not only the force and the displacements were considered as nodal variables, but also the Young's modulus and the Poisson's ratio. Although such work presents original and potentially promising concepts for the mechanical characterization of VPs, this approach suffers from two major limitations. First, the standard spatial shape functions used are continuous and therefore do not allow to characterize anatomical heterogeneous atherosclerotic lesions exhibiting high material discontinuities between inclusions. Second, despite its numerical robustness, this iterative method still remains time-consuming for high definition reconstruction elasticity map.

The present theoretical study was therefore designed to develop a FE method-based direct computational algorithm for elasticity reconstruction problems which accounts for material discontinuities. This new algorithm was obtained by extending the nodal material properties (NMP) approach proposed by Oberai *et al* (2003). To model material discontinuities between FEs, we modified and adapted the extended FE (Xfem) method (Moës *et al* 1999) to the NMP approach. Xfem method is a based FE approximation enriched by the addition of shape functions and used mainly in crack analysis (Moës *et al* 1999). This new direct atherosclerotic plaque elasticity reconstruction method, based on the original material-FE formulation allowing for material discontinuities (named *NMP-Xfem*⁻¹), was applied to six coronary lesions of patients imaged *in vivo* with IVUS. The sensitivity of NMP-Xfem⁻¹ method was characterized with regard to noise which affects the elasticity map reconstruction.

2. Material and methods

Six patients underwent coronary IVUS, and the extracted plaque geometries were used to simulate displacement and strain fields from which the performance of the original direct elasticity reconstruction method NMP-Xfem⁻¹ was tested.

2.1. IVUS study and plaque geometries

2.1.1. Patient population—Arteries were explored in patients referred for percutaneous coronary intervention at the Lyon Cardiology Hospital (Hôpital Cardiologique et Pneumologique de Lyon, France) after a first ACS with troponin I elevation. Investigations were approved by the institutional board of the Hospital Cardiology Department and patients consent.

2.1.2. Intravascular ultrasound imaging—Non-ruptured VP geometries were obtained from IVUS scans of the coronary arteries following the protocol described by Rioufol *et al* (2002). IVUS scans were performed with an iLab platform (Boston Scientific, Watertown, MA) equipped with 40 MHz catheters (Atlantis SR Pro 3.6F, Boston Scientific). The spatial resolution of the ultrasound images acquired with the IVUS system was approximately 90 μm in the radial direction (Chopard *et al* 2010).

2.1.3. IVUS image analysis—IVUS echogenecity aspects were used to characterize VP components (Di Mario *et al* 1998). A manual segmentation procedure using ImageJ software (ImageJ, NIH, Bethesda, MD, USA) was performed by a cardiologist to extract the contours of each plaque component.

2.1.4. IVUS measurements and definitions—Each IVUS image of a lesion was quantitatively analyzed. Measurement were made for plaque area (Pla_{area} , mm^2), lumen area (Lu_{area} , mm^2), necrotic core area ($Core_{area}$, mm^2), calcified area (Cal_{area} , mm^2), degree of stenosis ($Stenos_{deg}$, %) as $100 \times Pla_{area} / (Pla_{area} + Lu_{area})$ and cap thickness (Cap_{thick} , mm), which was defined as the shortest distance between the lumen and the necrotic core.

2.2. Solving the forward problem by using a material-FE formulation allowing for material discontinuities: simulated displacement fields

For the purpose of this study, atherosclerotic plaque components were modeled as isotropic and quasi-incompressible media with a linear elastic behavior. The FE models were solved under the assumption of plane strain. The two-dimensional proposed algorithm was derived by using the standard based displacement FE method. To account for material heterogeneities we introduced the notion of discontinuous nodal enrichment as performed to model failure in structural analysis. Based on such spirit, we originally adapted the extended FE method Xfem (Moes *et al* 1999) and implemented it into the material FE formulation proposed by Oberai *et al* (2003).

In order to introduce the notion of material discontinuous enrichment, we present the approach by considering the simple case of a plate made of three distinct media and meshed with four 4-node square FEs (figure 1). The Galerkin FE representation of the governing elasticity equations applied to this structure is given in matrix form by (Bathe 1982):

$$[K(\lambda, \mu)] \{U\} = \{F\} \quad (1)$$

where $\{F\}$ and $\{U\}$ are the nodal force and displacement vectors, respectively, and λ and μ are the Lamé's coefficient associated to the material properties of the FE, and $[K]$ is the global symmetric stiffness matrix. The displacement FE approximation are associated to regular mesh presented in figure 1(A) and are given by:

$$u(\vec{x}) = \sum_{i \in I} u_i \phi_i(\vec{x}) \quad (2a)$$

and

$$v(\vec{x}) = \sum_{i \in I} v_i \phi_i(\vec{x}) \quad (2b)$$

where u and v are the two components of the displacement vector, u_i and v_i are the displacements at node i , ϕ_i is the shape function associated with node i and \vec{x} is the position vector. The key issues of such technique are the selection of the appropriate nodes to enrich,

and the form of the associated enrichment shape functions. The nodal enrichment approach allows to satisfy the material discontinuity constraint by introducing additional nodes which increases the degree of freedom related to nodal material variables. We adopted the convention that a node must be enriched if it is located at the boundary of material discontinuities. Figure 1(B) illustrates the application of this rule. Nodes #2,4,5 and 6 were enriched. As a consequence, the FE approximation of the two material constants (i.e. the two Lamé's coefficients λ and μ of the FE) associated with the mesh in figure 1(B) is:

$$\lambda(\vec{x}) = \sum_{i \in J} \lambda_i \psi_i(\vec{x}) \quad (3a)$$

and

$$\mu(\vec{x}) = \sum_{i \in J} \mu_i \psi_i(\vec{x}) \quad (3b)$$

where I is the FE number, I is the set of all the nine initial nodes (i.e. before the enrichment process, $I = \{\text{nodes \# 1 to 9}\}$, see figure 1 (A)), J is the set of all the 14 nodes after the enrichment process (i.e. $J = \{\text{nodes \# 1 to 18 excluding nodes \# 2,4, 5 and 6}\}$, see figure 1(B)) and λ_k, μ_k ($k \in I, J$) are the components of the nodal material vectors $\{\lambda\}$ and $\{\mu\}$, respectively. Where shape functions φ_i ($i \in I$ and ψ_i ($i \in J$)) were used for displacement and material property fields, respectively. This material-FE formulation allowing for material discontinuities (named *NMP-Xfem*) was used to solve the forward problem.

2.2.1. Geometries—The files of the digitized contours obtained with ImageJ were imported into MATLAB. The entire plaque geometries were meshed with approximately 5000 3-Node triangular elements. The center of gravity of the lumen was used as the origin of the cylindrical coordinate system (r, θ).

2.2.2. Boundary conditions and material properties—Because instantaneous pressure was not recorded during the IVUS scans of the coronary arteries, we assumed a blood pressure differential P of 1 kPa (or 7.5 mmHg) which corresponds to a realistic pressure gradient occurring between two successive IVUS images recorded during the cardiac cycle. Free boundary condition was assumed at the external diameter of the artery. The mechanical properties of the arterial wall, fibrosis, soft necrotic core and calcified area were modeled as isotropic and quasi-incompressible media (Poisson ratio $\nu = 0.499$) with Young's moduli $E_{\text{wall}} = 150$ kPa, $E_{\text{fibrosis}} = 500$ kPa, $E_{\text{core}} = 5$ kPa and $E_{\text{calci.}} = 5000$ kPa, respectively (Finet *et al* 2004). All simulations were performed with the previous mechanical properties and with a blood pressure differential P of 1 kPa unless otherwise stated. The displacement and strain fields obtained with NMP-Xfem algorithm were used to test the performance of the original direct elasticity reconstruction methods proposed NMP-Xfem⁻¹.

2.2.3. Sensitivity study with regard to noise on input strain data—To investigate the influence of the noise on the performance of our direct elasticity reconstruction

technique, a white-noise was added to radial (ε_{rr}), circumferential ($\varepsilon_{\theta\theta}$) and shear ($\varepsilon_{r\theta}$) FE simulated strain fields used as inputs. To model the noise, we used a normal distribution of noise with zero mean and a standard deviation of $(a\varepsilon_{ij} + b)\beta$, with $a = 0.2\%$, $b = 0.04\%$ and where ε_{ij} is the local value of the strain (Baldewsing *et al* 2005, Le Floc'h *et al* 2009). The noise field was amplified by increasing β from 10^{-4} to 10^{-2} . For each level of noise β , 50 computations in which the noise was spatially randomly distributed were performed and we averaged the results obtained from these reconstructions.

The importance of considering a standard regulatory elasticity constraint to minimize the influence of white noise on the reconstructed elasticity map was also investigated. The constraint used requires that the Young's modulus of node ' k ' (E_k) must be equal to the mean Young's modulus of the two closest nodes ' $k+1$ ' and ' $k-1$ ': $E_k = (E_{k+1} + E_{k-1})/2$.

2.3. Solving the inverse problem by using a direct elasticity reconstruction method allowing for material discontinuities

2.3.1. FE formulation—Taking advantage of the linear relationships between the nodal displacement and material variables, we reformulated the equations of the forward FE methodology NMP-Xfem to obtain the linear FE formulation of the inverse algorithm NMP-Xfem⁻¹. We extracted a matrix $[Q]$ (named displacement matrix) that was used to solve for the nodal mechanical properties $\{R\}$. We thus obtained the following set of linear equilibrium equations for the new linear inverse FE methodology:

$$[Q(u_k, v_k)] \{R\} = \{F\} \quad \text{with} \quad \{R\} = \begin{bmatrix} \{\lambda\} \\ \{\mu\} \end{bmatrix} \quad (4)$$

The analytical expression of the FE rectangular displacement matrix $[Q_e]$ was derived for a two-dimensional plane strain triangular 3-node FE. To obtain the global displacement matrix $[Q]$, we assemble the FE displacement matrices exactly as it is performed for the standard displacement-FE method when deriving the global stiffness matrix $[K]$.

2.3.2. Numerical resolution—The global displacement matrix $[Q]$ is rectangular while the stiffness matrix $[K]$ is square. Both matrices $[Q]$ and $[K]$ have a same number of rows but their number of columns differs. The number of columns of $[Q]$ is equal to its number of rows plus two times the number of additional nodes considered at the level of the enriched nodes. Notice that a similar system can be obtained when using nodal strains instead of nodal displacement variables. Considering the inverse problem, the matrix $[Q]$ is known since all nodal displacements u_k and v_k are given. The inverse problem is ill conditioned because the nodal forces are not known on the nodes where the displacements were imposed. The global force vector $\{F\}$ has therefore some unknown components. By removing equations involving these unknown force components from the global FE system we obtained the following reduced system of linear equations:

$$[Q'] \{R\} = \{F'\} \quad (5)$$

where $\{F'\}$ and $[Q']$ denote the reduced nodal vector force and displacement matrix, respectively. To solve such linear rectangular system, we first transform it to a square system:

$$[Q']^T \{Q'\} \{R\} = [Q']^T \{F'\} \quad (6)$$

and then solve for the global NMP $\{R\}$:

$$\{R\} = ([Q']^T [Q'])^{-1} [Q']^T \{F'\}. \quad (7)$$

This numerical approach was detailed, used and discussed by Zhu *et al* (2003) and Guo *et al* (2010) in their direct Young's modulus reconstruction methods assuming constant Young's modulus in each FE.

Since the current IVUS-elastogram techniques does not allow to extract all strain components, we tested the performance of the elasticity reconstruction method NMP-Xfem⁻¹ by using the strain fields obtained with the forward NMP-Xfem method.

2.4. Elasticity reconstruction quality index (ER_{index})

For each plaque an elasticity map was reconstructed. The elasticity fields resulting from the reconstructed methods could highlight sites with negative Young's modulus amplitudes. Such values are not physically admissible. Therefore, to analyze the performance of these inverse methods, we defined an elasticity reconstruction quality index (ER_{index}, per cent of total plaque area) for which the resulting Young's modulus is physically admissible (0% ER_{index} 100%).

3. Results

3.1. IVUS study

After extensive IVUS scanning, six vulnerable non-ruptured coronary atherosclerotic lesions were identified. The geometrical features of these six VPs scanned *in vivo* (plaques # I to VI) were summarized in table 1.

3.2. Validation of the new linear material-FE formulation used for the resolution of the forward problem

Both, the forward NMP-Xfem and inverse NMP-Xfem⁻¹ algorithms have been implemented with MATLAB software (MATLAB, version 7.6.0(R2008a), MathWorks, Natick, MA, USA). Results obtained with the forward NMP-Xfem method—used to simulate the input displacement and strain fields of the direct FE elasticity reconstruction method NMP-Xfem⁻¹—have been validated on plaque # I by comparing them with those obtained by using the commercially available COMSOL Multiphysics software (Structural Mechanics Module, version 3.5, COMSOL, Grenoble, France). The amplitudes of the highest nodal relative absolute variations obtained on displacement and strain fields were lower than 5%.

3.3. Performance of the direct FE elasticity reconstruction method NMP-Xfem⁻¹

All results presented in our figures were obtained from simulations performed without white noise unless otherwise stated.

3.3.1. Importance of considering the enriched nodes approach when solving the inverse problem—

Two types of FE simulations were performed to highlight the importance of using the modified extended FE method Xfem for the resolution of the inverse problem. At first, the elasticity reconstruction problem was solved with NMP-Xfem⁻¹ algorithm, whereas the second series of simulations were conducted without considering the modified-Xfem method. The latter algorithm was called NMP⁻¹. These simulations were performed on all studied atherosclerotic lesions (plaques # I to VI). The results showed that the modified-Xfem method improved the quality of the reconstructed elasticity maps (figures 2–7). Indeed, our quantitative results demonstrated that the highest mean relative absolute errors (\pm standard deviation) of the reconstructed Young's moduli obtained for the arterial wall, fibrosis, necrotic core, and calcified regions decreased from $95.3 \pm 15.56\%$ (plaque #V), $98.85 \pm 72.42\%$ (plaque #V), $103.29 \pm 111.86\%$ (plaque # III) and $95.3 \pm 10.49\%$ (plaque # IV), respectively, to values smaller than $2.6 \times 10^{-8} \pm 5.7 \times 10^{-8}\%$ (i.e. close to the exact solutions) when considering the improved elasticity reconstruction technique NMP-Xfem⁻¹ instead NMP⁻¹ algorithm (figure 8).

3.3.2. Performance of the direct NMP-Xfem⁻¹ inverse method in characterizing vulnerable plaques with soft inclusions—

The reconstructed Young's modulus maps obtained for VPs with one (plaques # I and II, figures 2 and 3) and two (plaque # III, figure 4) necrotic cores are presented. The Young's moduli of the arterial wall, fibrosis and necrotic cores were accurately quantified using the elasticity reconstruction method NMP-Xfem⁻¹ with mean relative absolute errors smaller than $0.2 \times 10^{-8} \pm 0.2 \times 10^{-8}\%$.

3.3.3. Performance of the NMP-Xfem⁻¹ inverse method in characterizing vulnerable plaques with calcified inclusions—

The accuracy of the reconstructed Young's modulus map was also tested on two VP morphologies (plaques # IV and V) with isolated necrotic cores and calcified inclusions (figures 5 and 6). The Young's moduli of the arterial wall, fibrosis, necrotic core and calcified inclusion were quantified with mean relative absolute errors smaller than $2.1 \times 10^{-8} \pm 5.6 \times 10^{-8}\%$. Figure 7 illustrates the performances of the proposed inverse material-FE method to quantify the elasticity of a complex VP (plaque # VI) with adjacent soft and hard inclusions located between 7 and 9 o'clock and one isolated large necrotic core located between 2 and 6 o'clock. Our results shown that NMP-Xfem⁻¹ methods quantifies the mechanical properties of the isolated soft inclusion adjacent to the calcified area with a mean relative absolute error lower than $2.6 \times 10^{-8} \pm 5.7 \times 10^{-8}\%$.

3.3.4. Influence of white noise on NMP-Xfem⁻¹ elasticity reconstruction technique—

The sensitivity of NMP-Xfem⁻¹ elasticity reconstruction technique when increasing the white noise level is presented in figure 9. The influence of white noise was studied on plaque # I. According to the performed simulations, this approach appears to be highly sensitive to the white noise level. The mean nodal relative absolute error of the

reconstructed Young's modulus for the necrotic core increased from $2.3 \pm 3.2\%$ with a white noise of $\beta = 10^{-4}$ to $95.0 \pm 98.2\%$ with a white noise of ($\beta = 8 \times 10^{-3}$) (figure 9). To give a physical meaning to the parameter β , we converted our white noise amplitude (droved by the parameter β) in dB-scale based on the definition of the signal-to-noise ratio (see the appendix). We found that $\beta = 10^{-4}$, 10^{-3} and 10^{-2} corresponds to noise levels of 100.2 dB, 80.2 dB and 60.2 dB, respectively.

3.3.5. Importance of considering an elasticity regulatory constraint for

material reconstruction problem—To reduce the influence of white noise an elasticity regulatory constraint (described in section 2.2.4) was introduced. It was demonstrated that for any plaque constituents (i.e. arterial wall, fibrosis, necrotic core or calcified area) and for any level of white noise (i.e. between $\beta = 10^{-4}$ to 8×10^{-3}), the elasticity reconstruction quality indexes ER_{index} reached 100% (i.e. that all Young's modulus values were found positive) when the regulatory constraint was taken into account. Notice that despite the use of such a regulatory constraint, the algorithm remains very sensitive to the level of white noise (figure 9, row 2) since for a noise level of $\beta = 8 \times 10^{-3}$ the mean relative absolute errors for the arterial wall, fibrosis and necrotic core exceeded $80.7 \pm 0.7\%$, $78.9 \pm 0.7\%$ and $78.75 \pm 1.61\%$, respectively.

3.3.6. CPU-time required to reconstructed a modulogram—Additional simulations were conducted in order to compare CPU-time when reconstructing the modulograms by either considering the proposed direct NMP-Xfem⁻¹ method or iterative iMOD approach of Le Floc'h *et al* (2009).

The iterative plaque elasticity reconstruction algorithm iMOD is based on a segmentation-driven optimization procedure and may take several minutes for high definition reconstructed elasticity maps. Such algorithm uses two time-consuming steps: (1) a pre-conditioning model to extract the plaque morphology (i.e. the number n of plaque inclusions) in order to initiate the optimization process, and (2) an approach combining a dynamic segmentation method with an optimization procedure to highlight the modulogram of the atherosclerotic plaque. More refined segmentations were obtained from the dynamic segmentation method by increasing the number n of plaque inclusions. The increase of pre-conditioning sites took into account smaller changes in Young's modulus. So, at the early stage of the dynamic segmentation procedure, the most abrupt changes in Young's modulus were taken into account and then progressively minor changes were considered. Thus, when a Young's modulus set solution has been obtained for a given number of pre-conditioning regions, the next iteration of the watershed segmentation procedure was started. The dynamic segmentation procedure was initiated with one region (i.e., $n = 1$).

To provide a fair CPU-time comparison between iMOD and NMP-Xfem⁻¹ methods, the CPU-time necessary to perform the step 1 was not recorded (i.e. the VP morphology was supposed to be known). These simulations were performed on a VP geometry imaged *in vivo* (plaque # IV). Our results demonstrated that for any plaque inclusions n for which the Young's modulus needs to be estimated, the direct inverse NMP-Xfem⁻¹ algorithm appears to be much faster than the iterative iMOD method (see table 2).

4. Discussion

Quantification of material composition (i.e. modulogram) and morphology of the atherosclerotic plaque components are the critical keys in detection of VPs (Cheng *et al* 1993, Finet *et al* 2004). Such knowledge are important in preventing and managing ACS (Libby 2001). As an alternative to modulography, a few groups investigated the use of shear wave elasticity imaging for normal vessel wall or plaque characterization (Couade *et al* 2010, Allen *et al* 2011). One should note, however, that this method relies on an extracorporeal probe capable of inducing acoustic radiation pressure, which is currently not amenable for IVUS coronary scan.

To account for the anatomical heterogeneity of the biological tissues, Oberai *et al* (2003) developed an iterative elasticity reconstruction method based on an original material-FE formulation. However, the spatial shape functions used did not allow to reconstruct the elasticity of atherosclerotic lesions exhibiting high material discontinuities between inclusions. Therefore, in the current study, the native material-FE approach was successfully revisited and extended not only to characterize all intraplaque inclusions in real time clinical use, but more importantly, to improve significantly the accuracy of the resulting elasticity map. The performance of the proposed elasticity reconstruction method was found similar to any of the vulnerable plaque geometry considered in this study. This performance was directly linked with the radial resolution close to 36 μm used in our mesh grid, which was adapted to the resolution of the Lagrangian speckle model estimator (LSME) method developed by Maurice *et al* (2007) to compute the radial strain field.

4.1. Is the radial strain elastogram sufficient to detect a vulnerable plaque?

Fibrous cap thickness is often used by interventional cardiologists to diagnose the degree of VP instability. Other emergent biomechanical factors such as necrotic core thickness—rather than necrotic core area—and arterial remodeling index were also found to be critical in determining plaque instability (Ohayon *et al* 2008, Cilla *et al* 2012). Ophir and colleagues (Ophir *et al* 1991, Cespedes *et al* 1993) were the pioneers on developing imaging techniques based on the strain field. Several IVUS strain reconstructions (de Korte *et al* 2002, Maurice *et al* 2007) and palpography methods (Cespedes *et al* 2000, Schaar *et al* 2003, Deleaval *et al* 2013) were developed to investigate atherosclerotic coronary artery plaques and to predict their vulnerability to rupture. Such techniques allowed the calculations of intraplaque radial strain images during the cardiac cycle. Detection of VP was based on the idea that the radial strain amplitude in soft inclusion regions (i.e. the lipid core) should be much larger than those in stiff inclusions (i.e. calcified and fibrosis areas) in response to blood pressure changes (de Korte *et al* 2002). However, radial strain elastograms are not sufficient to diagnose accurately the degree of vulnerability of an atherosclerotic lesion. Figure 3 clearly demonstrates such limitation. The measurable radial strain map of plaque # II (figure 3(B)) highlights a high strain site located at the endoluminal layer between 9 and 10 o'clock. The strain field alone seems to indicate that the plaque is vulnerable and unstable with the possibility of a necrotic core close to the lumen. However, the large size of the necrotic core and the fibrous cap thickness cannot be predicted from such radial strain elastogram (figure 3(B)).

4.2. Necessity to use prior geometrical information to solve the inverse problem

The main issue for improving the resolution of the inverse problem relies not only on the improvement of the mathematical optimization algorithm itself, but also on the preconditioning of the algorithm based on the best estimation of the plaque components' contours. Indeed, *a priori* information is imperatively needed to constrain the resolution of the inverse problem so that a unique reconstructed elasticity map could be found from the measured strain/displacement fields (Richards and Doyley 2011, Doyley 2012). Several studies (Beattie *et al* 1998, Khalil *et al* 2006) used medical images to manually approximate the atherosclerotic plaque morphology so that the contours of the heterogeneities were already known before the reconstruction process. Let us point out that a more accurate and fully automatic segmentation criterion was proposed by our group (Le Floch *et al* 2009) to detect plaque heterogeneities based on strain measurements. The potential of such original segmentation procedure was demonstrated in a previous *in vitro* experimental study conducted on vessel phantoms (Le Floch *et al* 2010), and more recently *in vivo* on human (Le Floch *et al* 2012).

4.3. Performance of the new elasticity reconstruction method NMP-Xfem⁻¹

We clearly demonstrated that the material-FE method NMP⁻¹ was unable to quantify accurately the mechanical properties of plaque components. Such approach tends to underestimate the Young's modulus amplitude of all plaque constituents (up to a factor twenty for arterial wall, necrotic core and calcified inclusion of plaques # I, III and IV, respectively) (figure 8). The NMP⁻¹ algorithm used continuous FE spatial shape functions which tend to smooth the spatial elasticity distribution and are therefore mainly responsible for such inaccurate results. When using the new elasticity reconstruction method NMP-Xfem⁻¹ allowing for material discontinuities, the computed Young's modulus values of all atherosclerotic plaque components were found with relative absolute errors smaller than 10⁻⁷% (i.e. close to the exact solutions). These results highlight also the performance of the numerical method used to solve the over-determined set of linear equations (7).

4.4. Characterizing the nonlinear mechanical properties

Most human tissue including coronary artery have a nonlinear stress-strain relationship (Holzapfel *et al* 2005). In this model we assumed the elastic behaviors of the plaque constituents to be linear. This assumption remains reasonable if we used the strain fields measured between two successive frames of an IVUS sequence. Notice that such technique may be used to characterize *in vivo* the nonlinear mechanical responses of atherosclerotic plaque components occurring in systolic and diastolic phases during which the blood pressure amplitude increases and decreases, respectively. For each patient's atherosclerotic lesion, approximately 30 elasticity maps could be reconstructed based on the IVUS sequence recorded during the cardiac period (i.e. 30 images s⁻¹). Interestingly, the incremental local variation of the Young's modulus computed between all two successive frames during the cardiac phase will reveal the nonlinear mechanical properties of the arteriosclerotic lesion under physiological loading. Such technique has been successfully tested and validated on an *in vitro* experimental study performed by our group on vessel phantoms in which we

showed that the strain hardening effect was partly responsible for the resulting significant increase of the computed Young's modulus (Le Floc'h *et al* 2010).

4.5. Study limitations

Several limitations deserve to be pointed out at this stage of our developments, even if the present study includes findings which may help to increase the performance of the atherosclerotic plaque elasticity reconstruction methods.

First, the proposed elasticity reconstruction technique NMP-Xfem^{-1} appears to be very sensitive to noise in the strain measurements. Such result was expected since the proposed algorithm is linear. To overcome such limitation, alternatives would have been: (1) to solve our current system of linear equations (7) by minimizing a functional using the numerical algorithm of Oberai *et al* (2003) based on their original efficient modified adjoint method. However such alternative would not have been real time clinical use, or (2) to develop a relevant strain-noise filters and specific elasticity constraints to improve the accuracy of the reconstructed elasticity maps.

A second important study limitation remains the necessity to measure all strain fields, including the shear strain field, for the reconstruction of plaque using the NMP-Xfem^{-1} method. However, Cloutier's group showed that the shear strain field could now also be estimated by using their improved LSME method (Majdouline *et al* 2011).

Finally, the influence of residual stresses (Matsumoto *et al* 2004), generated during plaque growth process, has been ignored in this study. Residual stress patterns have been extensively studied *ex vivo* in several human vulnerable coronary plaque samples (Ohayon *et al* 2007). Neglecting residual stresses in the elasticity reconstruction analysis could bias the mechanical stress quantification, but not the characterization of the mechanical properties, which was the main goal of this study.

4.6. Influence of material discontinuity on vulnerable plaque stability

Although past studies have identified $\text{Cap}_{\text{thick}}$ as the primary predictor of coronary plaque rupture, biomechanical studies have recognized PCS as an additional key predictor of plaque disruption (Loree *et al* 1992). Quantification of PCS amplitude requires not only an accurate description of plaque morphology but also a precise knowledge of the mechanical properties of plaque components. Complex coronary VPs are highly heterogeneous and such lesions present several material discontinuities. Material discontinuity between lipid-rich (or necrotic core) and fibrous regions is critical since it generates high tensile circumferential stress in the TCFA. This intraparietal PCS is mainly responsible for the biomechanical rupture of the vulnerable plaque. The influence of such material discontinuity on the elasticity reconstruction has been explored by our group in a previous work conducted on seven coronary atherosclerotic plaques of patients imaged *in vivo* with IVUS (Le Floc'h *et al* 2009). While the Young's moduli of the fibrous regions were accurately identified (with relative error of + 2%), those of the soft and hard inclusions were overestimated (with relative error of + 32%) and underestimated (with relative error of -43%), respectively (Le Floc'h *et al* 2009). Regarding the influence of the lipid/fibrosis material discontinuity on the

PCS amplitude, Finet *et al* (2004) showed that a change in the core's material properties from lipid-rich (with Young's modulus close to 1 kPa) to soft atheromatous (with Young's modulus close to 20 kPa) exponentially reduced the stress amplitude in the TCFA (see figure 3 of Finet *et al* 2004). Such results strengthen the idea that any drug therapies which modify the mechanical properties of the VP constituents by decreasing the gradient of elasticity between the lipid-rich and fibrous media will be a benefit to patients and will stabilize the VPs.

4.7. Potential clinical implications

Finet *et al* (2004) demonstrated that a very slight increase in the mechanical properties of plaque constituents, namely the hardening of the lipid necrotic core, can tilt a VP from instability to stability. This work is in agreement with several studies conducted to analyze the structural variation in the fibrous cap and necrotic core with specific drug treatments (e.g., all statins, angiotensin converting enzyme inhibitors, etc) revealing an enhancement in plaque stability (Libby *et al* 2002, Abela *et al* 2011, Yla-Herttuala *et al* 2011, Nozue *et al* 2012). Due to its performance, accuracy and real time capabilities, the proposed elasticity imaging technique could provide an original approach to analyze the evolution of the mechanical properties of atherosclerotic plaques during drug therapies.

Acknowledgments

This research was supported by a joint international program of the ANR (MELANII project # 09-BLANC-0423) and NSERC strategic grant #STPGP-381136-09. Flavien Deleaval held a doctoral fellowship from la Région Rhône-Alpes, France (2010–13). Adeline Bouvier held a doctoral fellowship from the French Ministry for Higher Education and Research (MENRT 2010–13).

Appendix. Converting our white noise in decibel (dB)

To find a correspondence between the imposed white noise and the signal-to-noise ratio SNR (unit: dB) we used the following relationship:

$$\text{SNR} = 10 \log_{10} \left(\frac{A_{\text{signal}}^2}{A_{\text{noise}}^2} \right) \quad (\text{A.1})$$

where A_{signal} and A_{noise} are the signal and noise amplitudes, respectively. We identified the signal amplitude A_{signal} to the mean spatial strain amplitude free of noise. Moreover, in our study, we used the following normal distribution of noise A_{noise} with zero mean and standard deviation $\sigma(r, \theta) = (a\varepsilon_{ij}(r, \theta) + b)\beta$ where $a = 0.2\%$, $b = 0.04\%$ and β varies from 10^{-4} to 10^{-2} (Baldewsing *et al* 2005, Le Floc'h *et al* 2009):

$$A_{\text{noise}}(r, \theta) = \text{Normal}(0, \sigma(r, \theta)^2). \quad (\text{A.2})$$

By considering these two expressions of A_{signal} and A_{noise} we found:

$$\text{SNR} = 10 \log_{10} \left(\frac{\sum_{r,\theta} [\varepsilon_{ij}(r, \theta)]^2}{\sum_{r,\theta} [A_{\text{noise}}(r, \theta)]^2} \right). \quad (\text{A.3})$$

References

- Abela GS, Vedre A, Janoudi A, Huang R, Durga S, Tamhane U. Effect of statins on cholesterol crystallization and atherosclerotic plaque stabilization. *Am J Cardiol.* 2011; 107:1710–7. [PubMed: 21507364]
- Allen JD, Ham KL, Dumont DM, Sileshi B, Trahey GE, Dahl JJ. The development and potential of acoustic radiation force impulse (ARFI) imaging for carotid artery plaque characterization. *Vasc Med.* 2011; 6:302–11. [PubMed: 21447606]
- Baldewijs RA, Mastik F, Schaar JA, Serruys PW, van der Steen AF. Robustness of reconstructing the young's modulus distribution of vulnerable atherosclerotic plaques using a parametric plaque model. *Ultrasound Med Biol.* 2005; 31:1631–45. [PubMed: 16344126]
- Bathe, KJ. *Finite Element Procedure in Engineering Analysis.* Englewood Cliffs, NJ: Prentice-Hall; 1982.
- Beattie D, Xu C, Vito R, Glagov S, Whang MC. Mechanical analysis of heterogeneous, atherosclerotic human aorta. *J Biomech Eng.* 1998; 120:602–7. [PubMed: 10412437]
- Briley-Saebo KC, Mulder WJ, Mani V, Hyafil F, Amirbekian V, Aguinaldo JG, Fisher EA, Fayad ZA. Magnetic resonance imaging of vulnerable atherosclerotic plaques: current imaging strategies and molecular imaging probes. *J Magn Reson Imaging.* 2007; 26:460–79. [PubMed: 17729343]
- Carlier SG, Tanaka K. Studying coronary plaque regression with IVUS: a critical review of recent studies. *J Interv Cardiol.* 2006; 19:11–5. [PubMed: 16483334]
- Céspedes EI, de Korte CL, van der Steen AF. Intraluminal ultrasonic palpation: assessment of local and cross-sectional tissue stiffness. *Ultrasound Med Biol.* 2000; 26:385–96. [PubMed: 10773368]
- Céspedes I, Ophir J, Ponnekanti H, Maklad N. Elastography: elasticity imaging using ultrasound with application to muscle and breast *in vivo* *Ultrason. Imaging.* 1993; 15:73–88.
- Cheng GC, Loree HM, Kamm RD, Fishbein MC, Lee RT. Distribution of circumferential stress in ruptured and stable atherosclerotic lesions. A structural analysis with histopathological correlation. *Circulation.* 1993; 87:1179–87. [PubMed: 8462145]
- Chopard R, Boussel L, Motreff P, Rioufol G, Tabib A, Douek P, Meyronet D, Revel D, Finet G. How reliable are 40 MHz IVUS and 64-slice MDCT in characterizing coronary plaque composition? An ex vivo study with histopathological comparison. *Int J Cardiovasc Imaging.* 2010; 26:373–83. [PubMed: 20052618]
- Cilla M, Pena E, Martinez MA. 3D computational parametric analysis of eccentric atheroma plaque: influence of axial and circumferential residual stresses. *Biomech Modeling Mechanobiol.* 2012; 11:1001–13.
- Couade M, Pernot M, Prada C, Messas E, Emmerich J, Bruneval P, Criton A, Fink M, Tanter M. Quantitative assessment of arterial wall biomechanical properties using shear wave imaging. *Ultrasound Med Biol.* 2010; 36:1662–76. [PubMed: 20800942]
- de Korte CL, Carlier SG, Mastik F, Doyley MM, van der Steen AF, Serruys PW, Bom N. Morphological and mechanical information of coronary arteries obtained with intravascular elastography; feasibility study *in vivo.* *Eur Heart J.* 2002; 23:405–13. [PubMed: 11846498]
- Deleaval F, Bouvier A, Finet G, Cloutier G, Yazdani SK, Le Floc'h S, Clarysse P, Pettigrew RI, Ohayon J. The intravascular ultrasound elasticity-palpography technique revisited: A reliable tool for the *in vivo* detection of vulnerable coronary atherosclerotic plaques. *Ultrasound Med Biol.* 2013; 39:1469–81. [PubMed: 23727295]
- Di Mario C, et al. Clinical application and image interpretation in intracoronary ultrasound. Study group on intracoronary imaging of the working group of coronary circulation and of the subgroup on intravascular ultrasound of the working group of echocardiography of the European society of cardiology. *Eur Heart J.* 1998; 19:207–29. [PubMed: 9519314]

- Doyley MM. Model-based elastography: a survey of approaches to the inverse elasticity problem. *Phys Med Biol*. 2012; 57:R35–73. [PubMed: 22222839]
- Doyley MM, Mastik F, de Korte CL, Carlier SG, Cespedes EI, Serruys PW, Bom N, van der Steen AF. Advancing intravascular ultrasonic palpation toward clinical applications. *Ultrasound Med Biol*. 2001; 27:1471–80. [PubMed: 11750745]
- Doyley MM, Meaney PM, Bamber JC. Evaluation of an iterative reconstruction method for quantitative elastography. *Phys Med Biol*. 2000; 45:1521–40. [PubMed: 10870708]
- Finet G, Ohayon J, Rioufol G. Biomechanical interaction between cap thickness, lipid core composition and blood pressure in vulnerable coronary plaque: impact on stability or instability. *Coron Artery Dis*. 2004; 15:13–20. [PubMed: 15201616]
- Fleg JL, et al. Detection of high-risk atherosclerotic plaque: report of the NHLBI working group on current status and future directions. *J Am College Cardiol Imaging*. 2012; 5:941–55.
- Guo Z, You S, Wan X, Bicanic N. A FEM-based direct method for material reconstruction inverse problem in soft tissue elastography. *Comput Struct*. 2010; 88:1459–68.
- Holzapfel GA, Sommer G, Gasser CT, Regitnig P. Determination of layer-specific mechanical properties of human coronary arteries with nonatherosclerotic intimal thickening and related constitutive modeling. *Am J Physiol Heart Circ Physiol*. 2005; 289:H2048–58. [PubMed: 16006541]
- Jang IK, et al. Visualization of coronary atherosclerotic plaques in patients using optical coherence tomography: comparison with intravascular ultrasound. *J Am College Cardiol*. 2002; 39:604–9.
- Kanai H, Hasegawa H, Ichiki M, Tezuka F, Koiwa Y. Elasticity imaging of atheroma with transcutaneous ultrasound: preliminary study. *Circulation*. 2003; 107:3018–21. [PubMed: 12810617]
- Khalil AS, Bouma BE, Kaazempur Mofrad MR. A combined FEM/ genetic algorithm for vascular soft tissue elasticity estimation. *Cardiovasc Eng*. 2006; 6:93–102. [PubMed: 16967325]
- Kim K, Weitzel WF, Rubin JM, Xie H, Chen X, O'Donnell M. Vascular intramural strain imaging using arterial pressure equalization. *Ultrasound Med Biol*. 2004; 30:761–71. [PubMed: 15219956]
- Larose E, et al. Characterization of human atherosclerotic plaques by intravascular magnetic resonance imaging. *Circulation*. 2005; 112:2324–31. [PubMed: 16203910]
- Le Floch S, Cloutier G, Finet G, Tracqui P, Pettigrew RI, Ohayon J. On the potential of a new IVUS elasticity modulus imaging approach for detecting vulnerable atherosclerotic coronary plaques: in vitro vessel phantom study. *Phys Med Biol*. 2010; 55:5701–21. [PubMed: 20826899]
- Le Floch S, Cloutier G, Saijo Y, Finet G, Yazdani SK, Deleaval F, Rioufol G, Pettigrew RI, Ohayon J. A four-criterion selection procedure for atherosclerotic plaque elasticity reconstruction based on in vivo coronary intravascular ultrasound radial strain sequences. *Ultrasound Med Biol*. 2012; 38:2084–97. [PubMed: 23196202]
- Le Floch S, Ohayon J, Tracqui P, Finet G, Gharib AM, Maurice RL, Cloutier G, Pettigrew RI. Vulnerable atherosclerotic plaque elasticity reconstruction based on a segmentation-driven optimization procedure using strain measurements: theoretical framework. *IEEE Trans Med Imaging*. 2009; 28:1126–37. [PubMed: 19164080]
- Libby P. Current concepts of the pathogenesis of the acute coronary syndromes. *Circulation*. 2001; 104:365–72. [PubMed: 11457759]
- Libby P, Ridker PM, Maseri A. Inflammation and atherosclerosis. *Circulation*. 2002; 105:1135–43. [PubMed: 11877368]
- Lloyd-Jones D, et al. Executive summary: heart disease and stroke statistics-2010 update: a report from the American Heart Association. *Circulation*. 2010; 121:948–54. [PubMed: 20177011]
- Loree HM, Kamm RD, Stringfellow RG, Lee RT. Effects of fibrous cap thickness on peak circumferential stress in model atherosclerotic vessels. *Circ Res*. 1992; 71:850–8. [PubMed: 1516158]
- Majdouline Y, Garcia D, Le Floch S, Roy Cardinal MH, Destrempes F, Ohayon J, Cloutier G. Shear strain endovascular elastography for characterizing atherosclerotic plaques: in vitro vessel phantom study. 3rd MICCAI Workshop on Computing and Visualization for (Intra) Vascular Imaging. 2011:23–30.

- Maldonado N, Kelly-Arnold A, Vengrenyuk Y, Laudier D, Fallon JT, Virmani R, Cardoso L, Weinbaum S. A mechanistic analysis of the role of microcalcifications in atherosclerotic plaque stability: potential implications for plaque rupture. *Am J Physiol Heart Circ Physiol*. 2012; 303:H619–28. [PubMed: 22777419]
- Matsumoto T, Goto T, Furukawa T, Sato M. Residual stress and strain in the lamellar unit of the porcine aorta: experiment and analysis. *J Biomech*. 2004; 37:807–15. [PubMed: 15111068]
- Maurice RL, Fromageau J, Brusseau E, Finet G, Rioufol G, Cloutier G. On the potential of the Lagrangian estimator for endovascular ultrasound elastography: in vivo human coronary artery study. *Ultrasound Med Biol*. 2007; 33:1199–205. [PubMed: 17466446]
- Maurice RL, Ohayon J, Finet G, Cloutier G. Adapting the Lagrangian speckle model estimator for endovascular elastography: theory and validation with simulated radio-frequency data. *J Acoust Soc Am*. 2004; 116:1276–86. [PubMed: 15376693]
- Moës N, Dolbow J, Belytschko T. A finite element methods for crack growth without remeshing. *Int J Numer Methods Eng*. 1999; 46:131–50.
- Nozue T, et al. Statin treatment for coronary artery plaque composition based on intravascular ultrasound radiofrequency data analysis. *Am Heart J*. 2012; 163:191–9. e1. [PubMed: 22305836]
- Oberai AA, Gokhale NH, Feijoo GR. Solution of inverse problems in elasticity imaging using the adjoint method. *Inverse Problems*. 2003; 19:297–313.
- Ohayon J, Dubreuil O, Tracqui P, Le Floch S, Rioufol G, Chalabreysse L, Thivolet F, Pettigrew RI, Finet G. Influence of residual stress/ strain on the biomechanical stability of vulnerable coronary plaques: potential impact for evaluating the risk of plaque rupture. *Am J Physiol Heart Circ Physiol*. 2007; 293:H1987–96. [PubMed: 17604326]
- Ohayon J, Finet G, Gharib AM, Herzka DA, Tracqui P, Heroux J, Rioufol G, Kotys MS, Elagha A, Pettigrew RI. Necrotic core thickness and positive arterial remodeling index: emergent biomechanical factors for evaluating the risk of plaque rupture. *Am J Physiol Heart Circ Physiol*. 2008; 295:H717–27. [PubMed: 18586893]
- Ohayon J, Teppaz P, Finet G, Rioufol G. *In-vivo* prediction of human coronary plaque rupture location using intravascular ultrasound and the finite element method. *Coron Artery Dis*. 2001; 12:655–63. [PubMed: 11811331]
- Ophir J, Cespedes I, Ponnekanti H, Yazdi Y, Li X. Elastography: a quantitative method for imaging the elasticity of biological tissues. *Ultrason Imaging*. 1991; 13:111–34. [PubMed: 1858217]
- Richards MS, Doyley MM. Investigating the impact of spatial priors on the performance of model-based IVUS elastography. *Phys Med Biol*. 2011; 56:7223–46. [PubMed: 22037648]
- Rioufol G, Finet G, Ginon I, Andre-Fouet X, Rossi R, Vialle E, Desjoyaux E, Convert G, Huret JF, Tabib A. Multiple atherosclerotic plaque rupture in acute coronary syndrome: a three-vessel intravascular ultrasound study. *Circulation*. 2002; 106:804–8. [PubMed: 12176951]
- Schaar JA, de Korte CL, Mastik F, Baldewsing R, Regar E, de Feyter P, Slager CJ, van der Steen AF, Serruys PW. Intravascular palpography for high-risk vulnerable plaque assessment. *Herz*. 2003; 28:488–95. [PubMed: 14569389]
- Tearney GJ, et al. Three-dimensional coronary artery microscopy by intracoronary optical frequency domain imaging. *J Am College Cardiol Imaging*. 2008; 1:752–61.
- Vancraeynest D, Pasquet A, Roelants V, Gerber BL, Vanoverschelde JL. Imaging the vulnerable plaque. *J Am College Cardiol*. 2011; 57:1961–79.
- Virmani R, Burke AP, Farb A, Kolodgie FD. Pathology of the vulnerable plaque. *J Am College Cardiol*. 2006; 47:C13–8.
- Virmani R, Kolodgie FD, Burke AP, Farb A, Schwartz SM. Lessons from sudden coronary death: a comprehensive morphological classification scheme for atherosclerotic lesions. *Arterioscler Thromb Vasc Biol*. 2000; 20:1262–75. [PubMed: 10807742]
- Wan M, Li Y, Li J, Cui Y, Zhou X. Strain imaging and elasticity reconstruction of arteries based on intravascular ultrasound video images. *IEEE Trans Biomed Eng*. 2001; 48:116–20. [PubMed: 11235583]
- Yla-Herttuala S, et al. Stabilisation of atherosclerotic plaques. Position paper of the European Society of Cardiology (ESC) working group on atherosclerosis and vascular biology. *Thromb Haemost*. 2011; 106:1–19. [PubMed: 21670845]

Zhu Y, Hall TJ, Jiang J. A finite-element approach for young's modulus reconstruction. IEEE Trans Med Imaging. 2003; 22:890–901. [PubMed: 12906243]

Author Manuscript

Author Manuscript

Author Manuscript

Author Manuscript

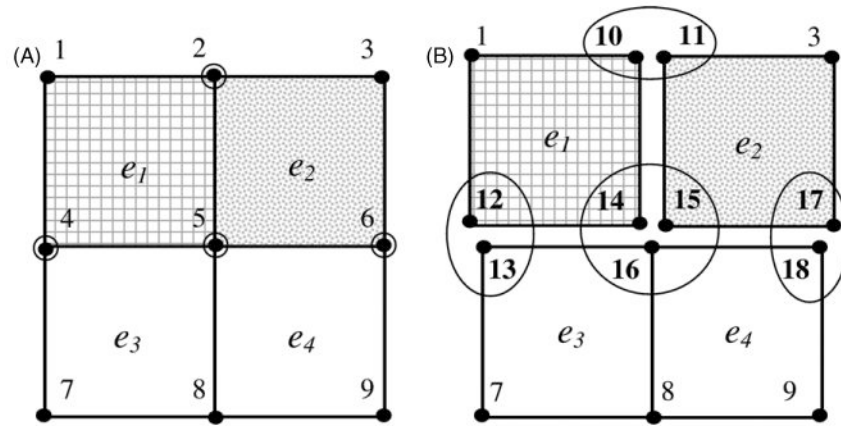


Figure 1.

(A) Regular mesh used for the FE approximations of displacements and forces. (B) Mesh used for the FE approximation of material properties. Nodes located at the lines of material discontinuities (i.e. nodes # 2, 4, 5 and 6 of mesh (A)) were enriched and replaced by the following sets of nodes (10, 11), (12, 13), (14, 15, 16) and (17, 18), respectively. The three media were illustrated by distinct colors. The circled nodes are the enriched nodes. e_i ($i = 1$ to 4) is the element number i .

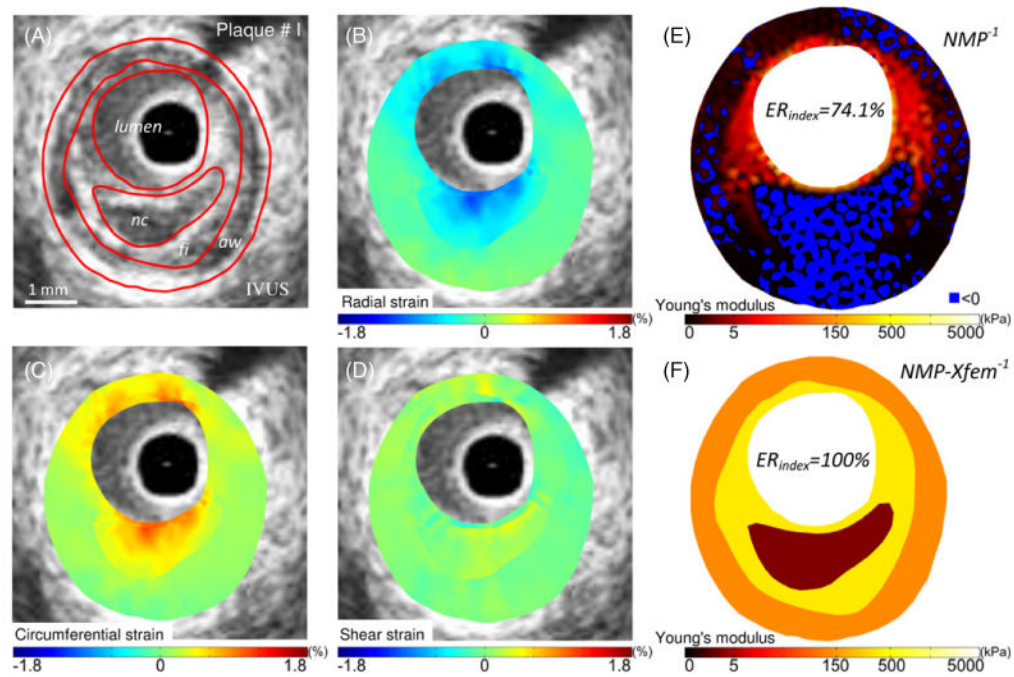


Figure 2.

Performance of the new direct atherosclerotic elasticity reconstruction method allowing for material discontinuities to detect a vulnerable plaque with one necrotic core. (A) IVUS image of plaque # I with plaque constituents (red contours, 'aw': arterial wall; 'fi': fibrous region; 'nc': necrotic core). (B) Radial strain field in the arterial cross-section. (C) Circumferential strain field in the arterial cross-section. (D) Shear strain field in the arterial cross-section. (E) Elasticity map reconstructed by using the NMP approach without the extended FE method Xfem allowing for material discontinuities (elasticity reconstruction method called NMP^{-1}). (F) Elasticity map reconstructed by including the extended FE method Xfem which account for material discontinuities (elasticity reconstruction method called $NMP-Xfem^{-1}$). ER_{index} is the elasticity reconstruction quality index which gives the per cent of total plaque area for which the computed Young's modulus is physically admissible.

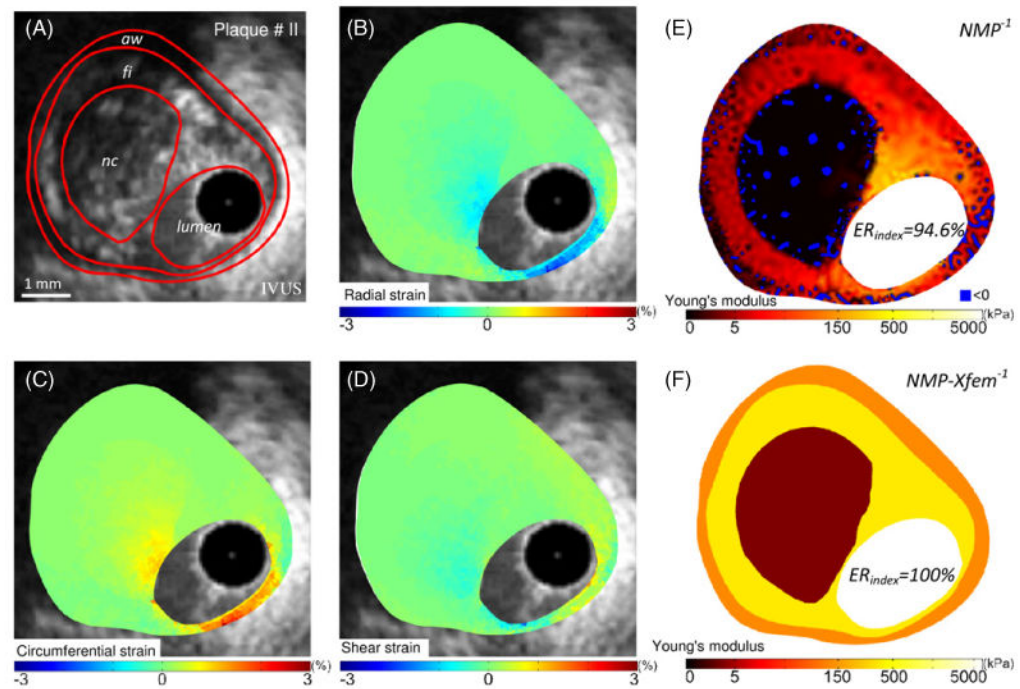


Figure 3.

Performance of the new direct atherosclerotic elasticity reconstruction method to characterize a vulnerable plaque with a large necrotic core. (A) IVUS image of plaque # II. (B) Radial strain. (C) Circumferential strain. (D) Shear strain. (E) Elasticity map reconstructed without the extended FE method Xfem. (F) Elasticity map reconstructed by including the extended FE method Xfem which account for material discontinuities.

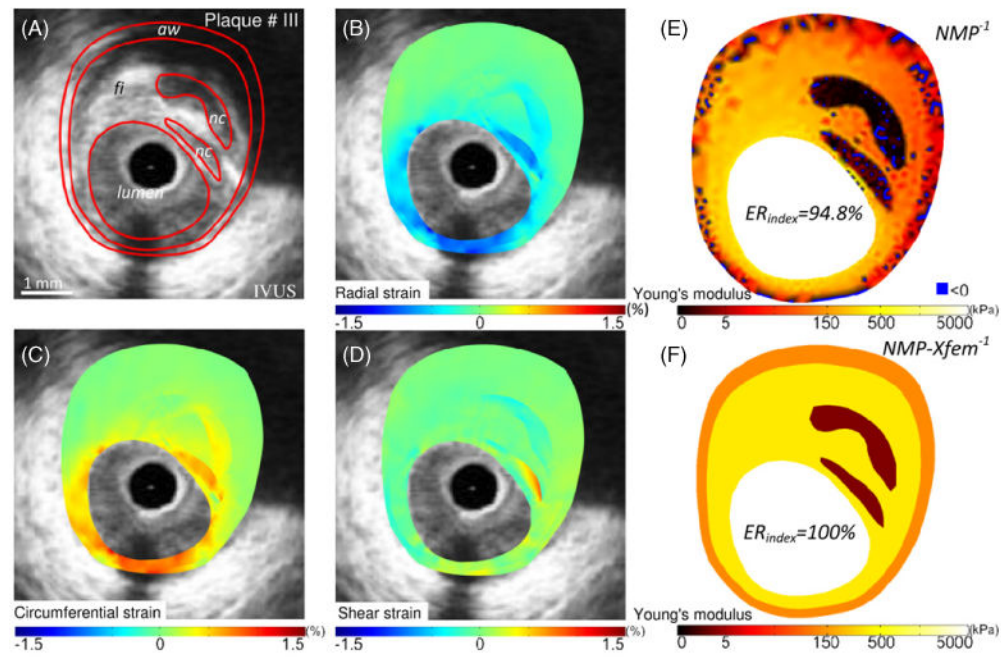


Figure 4.

Performance of the new direct atherosclerotic elasticity reconstruction method to characterize a vulnerable plaque with two necrotic cores. (A) IVUS image of plaque # III. (B) Radial strain. (C) Circumferential strain. (D) Shear strain. (E) Elasticity map reconstructed without the extended FE method Xfem. (F) Elasticity map reconstructed by including the extended FE method Xfem which account for material discontinuities.

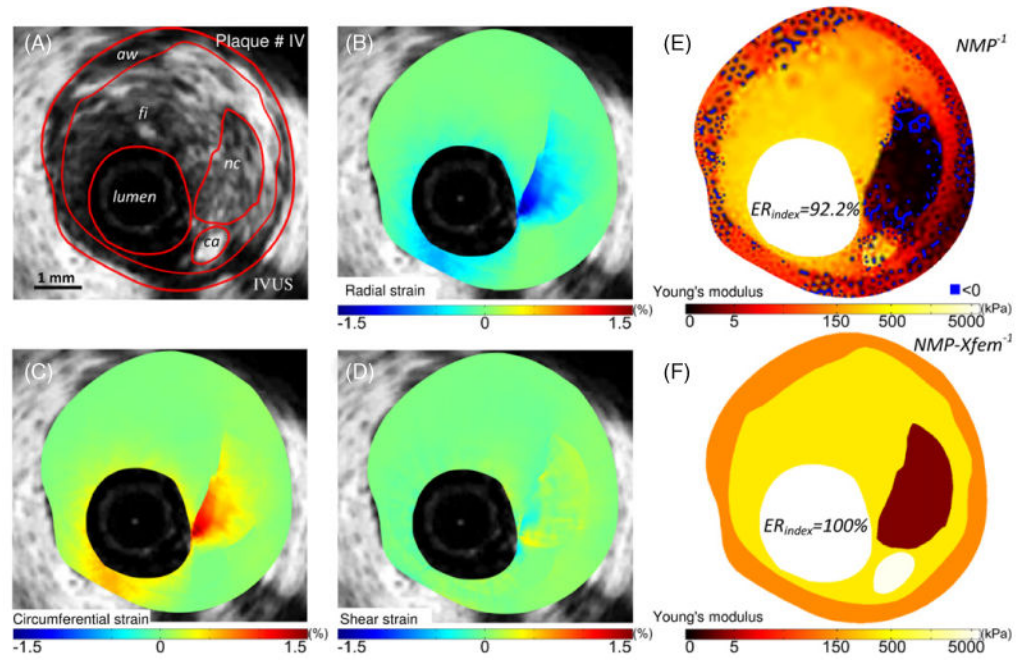


Figure 5.

Performance of the new direct atherosclerotic elasticity reconstruction method to characterize a vulnerable plaque with a small calcified inclusion. (A) IVUS image of plaque # IV. (B) Radial strain. (C) Circumferential strain. (D) Shear strain. (E) Elasticity map reconstructed without the extended FE method Xfem allowing for material discontinuities. (F) Elasticity map reconstructed by including the extended FE method Xfem which account for material discontinuities.

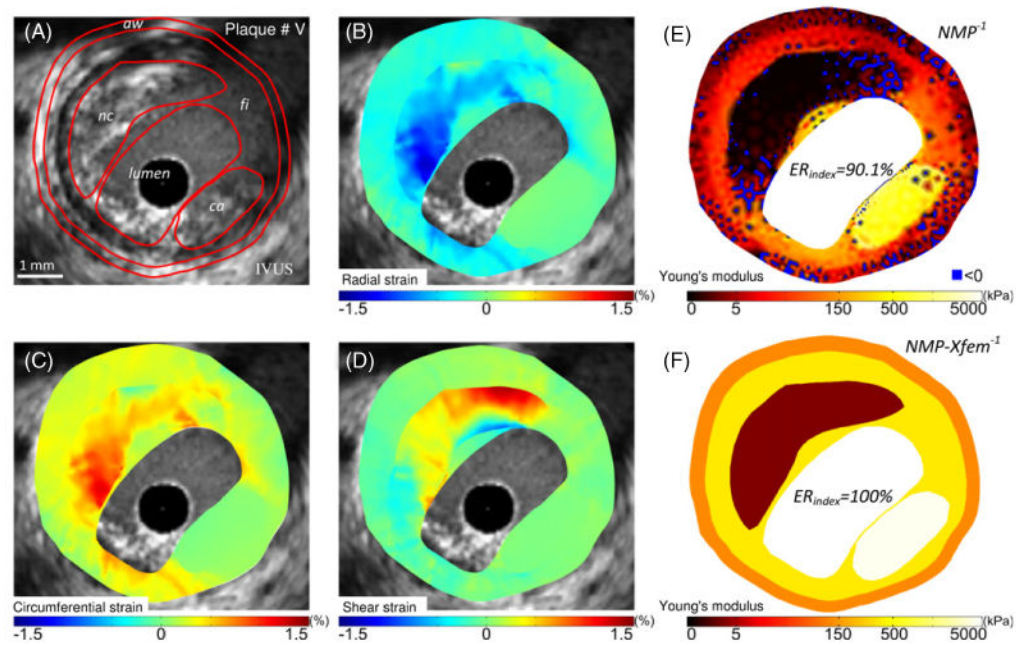


Figure 6.

Performance of the new direct atherosclerotic elasticity reconstruction method to characterize a vulnerable plaque with a large calcified inclusion. (A) IVUS image of plaque # V. (B) Radial strain. (C) Circumferential strain. (D) Shear strain. (E) Elasticity map reconstructed without the extended FE method Xfem. (F) Elasticity map reconstructed by including the extended FE method Xfem which account for material discontinuities.

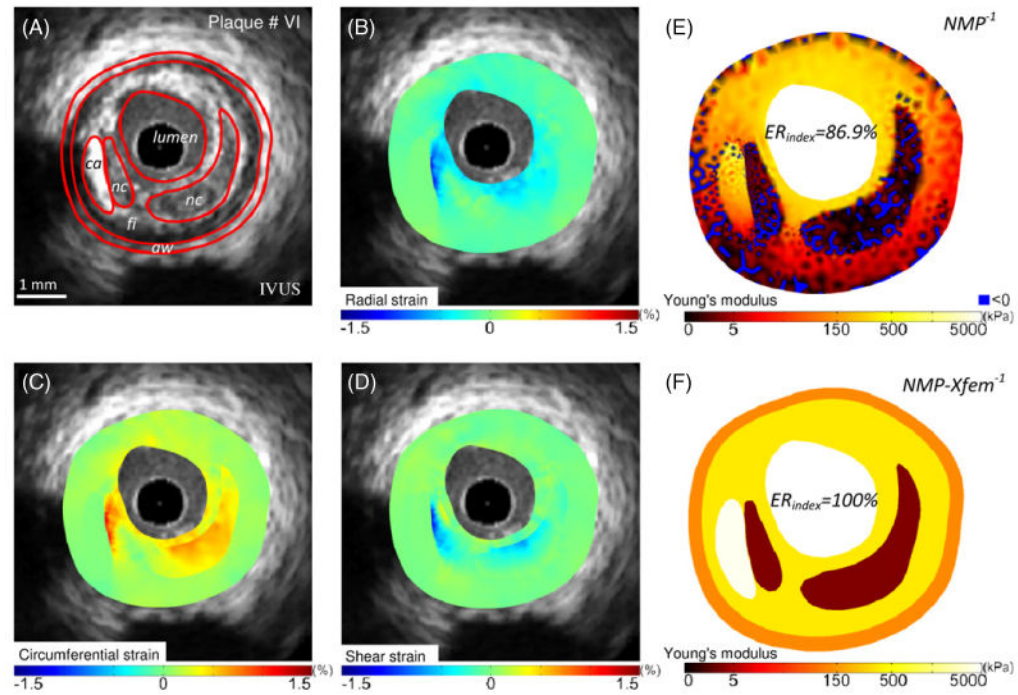


Figure 7.

Performance of the new direct atherosclerotic elasticity reconstruction method to characterize a vulnerable plaque with a small calcified inclusion adjacent to a necrotic core. (A) IVUS image of plaque # VI. (B) Radial strain. (C) Circumferential strain. (D) Shear strain. (E) Elasticity map reconstructed without the extended FE method Xfem. (F) Elasticity map reconstructed by including the extended FE method Xfem which account for material discontinuities.

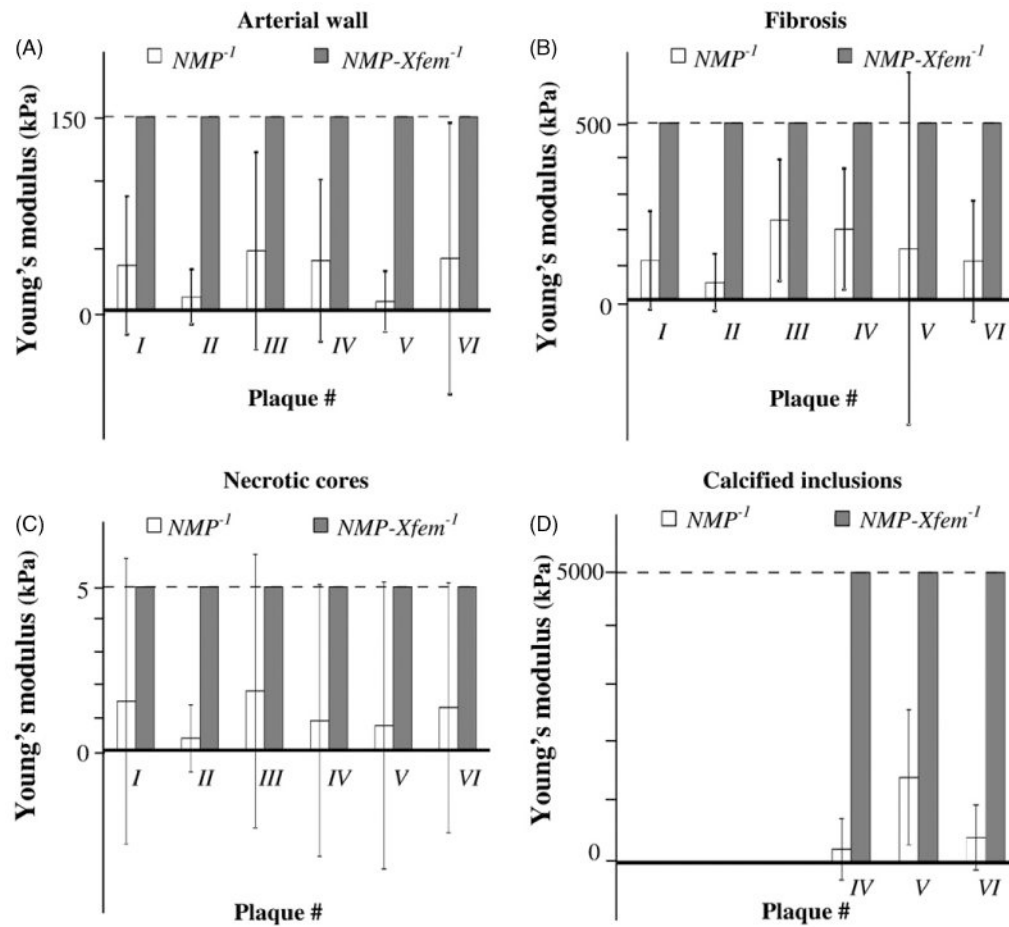


Figure 8. Estimation of the Young's moduli of the: (A) arterial wall, (B) fibrosis, (C) necrotic cores, and (E) calcified inclusions, when considering the elasticity reconstruction methods allowing ($NMP-Xfem^{-1}$) or not (NMP^{-1}) for material discontinuities.

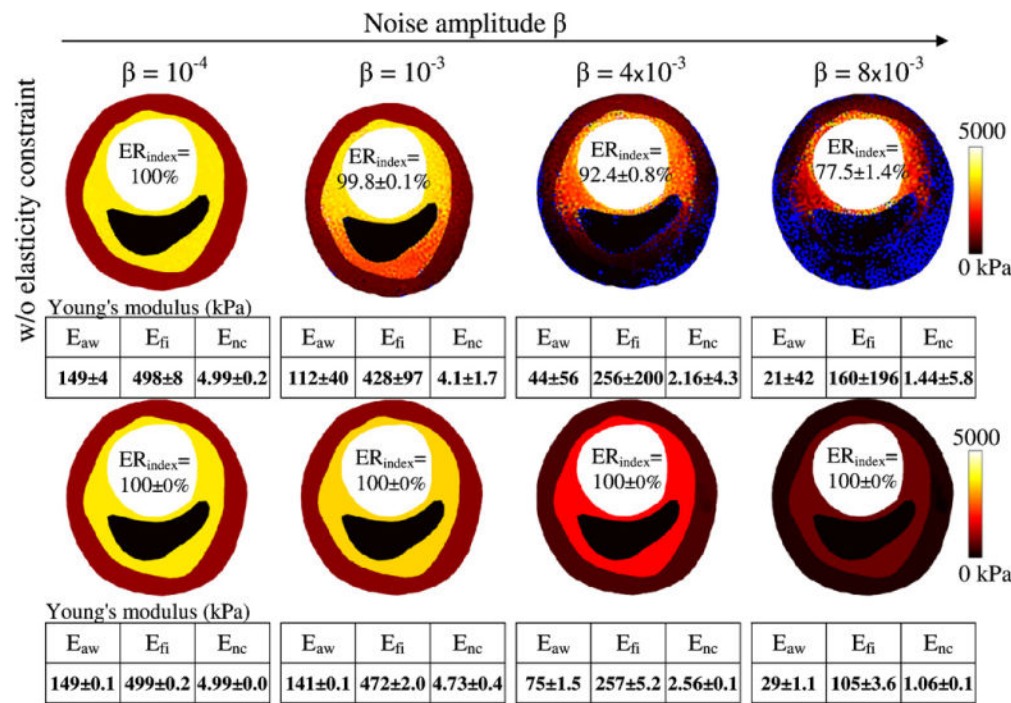


Figure 9. Results of the sensitivity analysis performed to investigate the influence of the white noise added to the strain fields on the reconstructed elasticity maps. Two types of simulations were conducted to highlight the importance of using a regulatory elasticity constraint for the resolution of the inverse problem. Plaque # I was used for this study. Column (1): reconstructed elasticity maps obtained with different level of white noise ($\beta = 10^{-4}$, 10^{-3} , 4×10^{-3} and 8×10^{-3}) when we neglected the regulatory elasticity constraint. Column (2): reconstructed elasticity maps obtained with different level of white noise when we considered the regulatory constraint. The amplitudes of the resulting mean Young's moduli of all plaque components and the elasticity reconstruction quality index ER_{index} obtained are given. Subscripts 'aw', 'fi' and 'nc' stands for arterial wall, fibrosis and necrotic core, respectively.

Table 1

Description of human coronary plaque characteristics detected *in vivo* by IVUS.

Plaque #	Cap thickness (mm)	Necrotic core areas (mm ²)	Calcified area area (mm ²)	Plaque area (mm ²)	Lumen area (mm ²)	Degree of stenosis (%)
I	0.093	1.36	–	8.74	2.79	76
II	0.100	5.39	–	16.70	3.24	84
III	0.162	1.20/0.51	–	17.85	6.75	73
IV	0.193	2.11	0.40	17.53	3.60	83
V	0.062	3.54	1.60	15.64	4.52	78
VI	0.220	2.15/0.70	0.89	16.88	3.62	82

Table 2

Recorded CPU-time for elasticity reconstruction maps conducted with the iterative method iMOD (Le Floc'h *et al* 2009) and with the proposed direct approach NMP-Xfem⁻¹.

Number of inclusions	iMOD (s)	NMP-Xfem ⁻¹ (s)	CPU-time ratio
$n = 10$	80	76	1.05
$n = 50$	620	106	5.85
$n = 100$	1160	154	7.53